

Article

Sparse Reconstruction of SFCWSAR Based on an Approximate Observation Operator

Xiaoze Hou and Yanheng Ma *

Unmanned Aerial Vehicle Engineering Department, Army Engineering University, Shijiazhuang 050051, China
* Correspondence: myh1472883699@163.com; Tel.: +86-15633167863

Abstract: The traditional compressed sensing SFCWSAR (Stepped Frequency Continuous Wave Synthetic Aperture Radar) sparse reconstruction algorithm consumes a lot of computer memory and cannot compensate the range migration in the same pulse group. Based on this, this paper proposes a SFCWSAR sparse reconstruction algorithm based on an approximate observation operator. First, the algorithm replaces the accurate observation operator with the approximate observation operator, which greatly reduces the computer memory consumption while the algorithm is running and realizes the compensation of the range migration in the SFCWSAR pulse group. Furthermore, the SFCWSAR sub-band echo data under full sampling conditions are used to modify the important parameter of the Doppler center frequency of the approximate observation operator, which significantly improves the reconstruction accuracy of the scene. The SFCWSAR data show that, compared with the conventional sparse autofocus algorithm, the proposed algorithm takes less memory and can reconstruct scenes with high accuracy.

Keywords: SFCWSAR; approximate observation operator; compression sensing

1. Introduction

A Synthetic Aperture Radar (SAR) can perform high-resolution imaging of long-range scenes throughout the day, in all weather. With the continuous growth of application requirements, people's demand for SAR high-resolution imaging is increasingly urgent [1–4]. However, the high resolution poses a great challenge to the instantaneous bandwidth and sampling rate of the radar system. SFCWSAR (Stepped Frequency Continuous Wave Synthetic Aperture Radar) can provide high-resolution imaging without increasing the radar's instantaneous bandwidth and sampling rate. The governing principle is to transmit multiple sub-bandwidth signals and synthesize the echo signals into a large-bandwidth signal through signal processing technology [5–8].

However, even if the SFCWSAR system is adopted, the amount of data that the system needs to process is not reduced in order to obtain the same resolution. This poses a great challenge to the memory and operation efficiency of the system, especially in the case of high-resolution imaging of wide-format scenes [9,10].

Compressed sensing theory shows that when the imaging scene meets the sparsity condition, the SAR image can be reconstructed with high precision with a small amount of radar echo data. Applying compressed sensing theory to SAR (Compressed Sensing Synthetic Aperture Radar, CS-SAR) can effectively reduce the amount of data to be processed and the pressure on the computer memory [11–14].

When SFCWSAR transmits one sub-pulse, the slant range between the radar and the target changes, and the change in the slant range during the sub-pulse transmission will inevitably affect the quality of the synthesized bandwidth. However, for the SFCWSAR radar system, the existing sparse reconstruction model cannot compensate the phase error of each sub-pulse in the same pulse group of SFCWSAR due to the relative motion between the radar and the target, which seriously reduces the imaging quality. Furthermore, the precise



Citation: Hou, X.; Ma, Y. Sparse Reconstruction of SFCWSAR Based on an Approximate Observation Operator. *Electronics* **2023**, *12*, 213. <https://doi.org/10.3390/electronics12010213>

Academic Editors: Lapo Miccinesi and Massimiliano Pieraccini

Received: 12 September 2022

Revised: 24 October 2022

Accepted: 24 October 2022

Published: 1 January 2023



Copyright: © 2023 by the authors. Licensee MDPI, Basel, Switzerland. This article is an open access article distributed under the terms and conditions of the Creative Commons Attribution (CC BY) license (<https://creativecommons.org/licenses/by/4.0/>).

observation matrix adopted by the existing sparse reconstruction model occupies too much computer memory, and the algorithm operation efficiency needs to be improved [15,16].

The team of the academician Wu Yirong from the Institute of Electronics, Chinese Academy of Sciences has proposed a sparse imaging method based on approximate observation operators through the research on traditional matched filter imaging algorithms. This method greatly reduces the dimension of the measurement matrix, reduces the computational load and memory footprint of the CS-SAR algorithm, and improves the computational efficiency of the algorithm; it has thus received extensive attention [17–19]. In addition, the approximate observation operator is derived from the traditional matched filter imaging algorithm. In this paper, it is applied to the sparse reconstruction of SFCWSAR, which makes it possible to compensate for the phase error of each sub-pulse in the same pulse group due to the relative motion of the radar and the target [20,21].

The above problem can be solved using an approximate observation operator instead of the existing precise observation matrix, and the construction of an approximate observation operator needs to obtain the accurate Doppler center frequency. However, the Doppler center frequency has errors because the carrier aircraft is easily affected by airflow and its mechanical vibration in the air. If the Doppler center frequency value obtained by theoretical calculation is directly used to construct the approximate observation operator, the theoretical model of imaging will not match the actual imaging process, which will seriously affect the sparse reconstruction [22,23]. Therefore, the Doppler center frequency needs to be estimated and compensated. The SAR carrier is generally equipped with a navigation and measurement system to detect the fast and slow variation of the antenna phase center and the in-plane and non-planar components of the disturbance and to compensate accordingly. However,

(1) Equipping with high-precision inertial navigation equipment increases the cost of the system hardware.

(2) Some flight platforms are unable to carry inertial navigation equipment with a large weight and volume due to load limitations, such as the SRUAV (Small Rotor Unmanned Aerial Vehicle).

Therefore, it is necessary to study data-driven Doppler centroid frequency estimation methods in consideration of the cost and load capacity of some SAR systems.

In view of the above problems, a sparse reconstruction algorithm based on the approximate observation operator SFCWSAR is proposed in this study. The algorithm compensates for the range migration within the pulse group and corrects the Doppler center frequency. In this method, the approximate observation operator is used to replace the precise observation operator, which not only improves the efficiency of scene reconstruction but also reduces the memory usage of the system. Then, the range migration within the SFCWSAR group is compensated, and the compensated echo data are used for the SFCWSAR sparse reconstruction. Furthermore, the narrowband sub-pulse signal under the full sampling condition is obtained through the construction of the sampling matrix, while the undersampled echo data is obtained. The Doppler center frequency is estimated using the complete narrowband echo signal. The approximate observation operator is modified using the estimated Doppler center frequency, and then the corrected approximate observation operator is used for the sparse reconstruction of the scene. The measured data show that the proposed algorithm can effectively reconstruct the scene with high precision and greatly improve the computational efficiency.

2. SFCWSAR Signal Model and Range Migration Correction in the Pulse Group

2.1. Stepped Frequency Continuous Wave SAR Signal Model

This section briefly introduces the signal model of SFCWSAR:

It is assumed that the sub-band pulse chirp bandwidth is B , the pulse length is T_{pn} , and the center frequency of each sub-pulse changes in steps of Δf . The center frequency of the broadband chirp signal obtained after narrowband sub-pulse synthesis is f_c , the bandwidth is B_n , and the pulse length is T_p .

The center frequency of the k th signal in the n narrowband pulse signals is:

$$f_c(k) = f_c + \left(k - \frac{1}{2} - \frac{n}{2}\right)\Delta f, (1 \leq k \leq n) \tag{1}$$

It is assumed that the radar transmits the K th signal of n narrowband pulse signals at time $t_{mk} = t_m + (k - 1)T_{pn}$, $1 \leq k \leq n$, the frequency modulation is K_r , and the range fast time is \hat{t} .

The transmitted signal is:

$$s(\hat{t}, k) = \text{rect}\left(\frac{\hat{t}}{T_{pn}}\right) \exp(j2\pi f_c(k)t) \exp(j\pi K_r \hat{t}^2) \tag{2}$$

Figure 1 shows the pulse waveform of the FM step frequency signal.

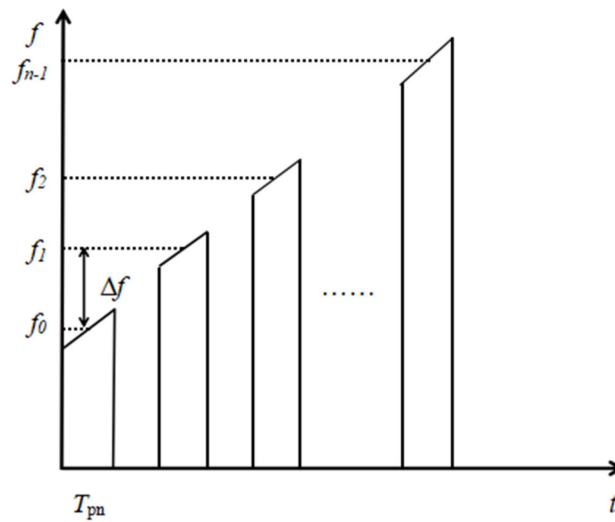


Figure 1. Pulse waveform of the Stepped Frequency Continuous Wave.

The target echo signal with distance R is:

$$S_r(\hat{t}, k) = \text{rect}\left(\frac{\hat{t} - 2R/c}{T_{pn}}\right) \exp(j2\pi f_c(k)(t - 2R/c)) \exp(j\pi K_r (\hat{t} - 2R/c)^2) \tag{3}$$

The reference function is:

$$S_{ref} = \exp(j2\pi f_c(k)\hat{t}) \tag{4}$$

Then, the received baseband signal is:

$$S_k(\hat{t}, R) = \text{rect}\left(\frac{\hat{t} - 2R/c}{T_{pn}}\right) \exp\left(-j\frac{4\pi}{c} f_c(k)R\right) \exp\left(j\pi K_r \left(\hat{t} - \frac{2R}{c}\right)^2\right) \tag{5}$$

2.2. Range Migration Correction in the Pulse Group

Section 2.1 briefly introduces the SFCWSAR signal. Different from other systems, SFCWSAR transmits multiple sub-bandwidth signals, and the echo signal is synthesized into a large-bandwidth signal through signal processing technology. During the transmission of each sub-pulse, the slant range between the radar and the target changes, and the change in the slant range during the transmission of the sub-pulse will inevitably affect the quality of the synthesized bandwidth.

It is assumed that the echo time delay of the target at distance R is τ_0 , there is relative motion between the radar and the target, and the relative radial velocity between the two

is v . If the above signal is not transmitted when the distance from the target is R and is delayed by T_r when the target distance is R , then the echo delay at this time is no longer τ_0 but:

$$\tau_p = \frac{2(R + vT_r)}{c} = \tau_0 + \tau_\Delta \tag{6}$$

τ_Δ indicates the time delay caused by the relative motion between the radar and target. Therefore, the echo at this time is no longer Equation (5) but becomes

$$S_k(\hat{t}, R) = \text{rect}\left(\frac{\hat{t} - \tau_0 - \tau_\Delta}{T_{Pn}}\right) \exp(-j2\pi f_c(k) \cdot (\tau_0 + \tau_\Delta)) \exp(j\pi K_r (\hat{t} - \tau_0 - \tau_\Delta)^2) \tag{7}$$

$$S_k(\hat{t}, R) = \text{rect}\left(\frac{\hat{t} - \tau_0 - \tau_\Delta}{T_{Pn}}\right) \exp(-j2\pi f_c(k)\tau_0) \exp(-j2\pi f_c(k)\tau_\Delta) \exp(j\pi K_r (\hat{t} - \tau_0 - \tau_\Delta)^2) \tag{8}$$

It can be seen from Equations (7) and (8) that there is an additional τ_Δ in the time domain and a constant phase term in the phase $\exp(-j2\pi f_c \tau_\Delta)$. The phase discontinuity and the time delay are caused by the relative motion between the radar and the target. These phases easily cause the target range to decrease in amplitude, the main lobe to widen, and even the divergence and distortion of the waveform. In order to improve the imaging quality of SFCWSAR, the phase error must be compensated.

For SFCWSAR, traditional sparse reconstruction algorithms based on precise observation operators cannot compensate for the above errors, resulting in a sharp decline in the quality of sparse reconstruction. In order to realize the compensation of the above phase error, the approximate observation operator is used in this paper instead of the precise observation matrix to realize the sparse reconstruction of SFCWSAR. It is possible to compensate for the range migration within the SFCWSAR pulse group because the approximate observation operator is derived from the imaging algorithm.

3. SFCWSAR Sparse Imaging Model Based on an Approximate Observation Operator

3.1. Approximate Observation Operator

According to a previous study, the specific principle analysis of the approximate observation operator is performed [24]. The approximate observation operator is shown in Figure 2. Let the undersampled echo data be S .

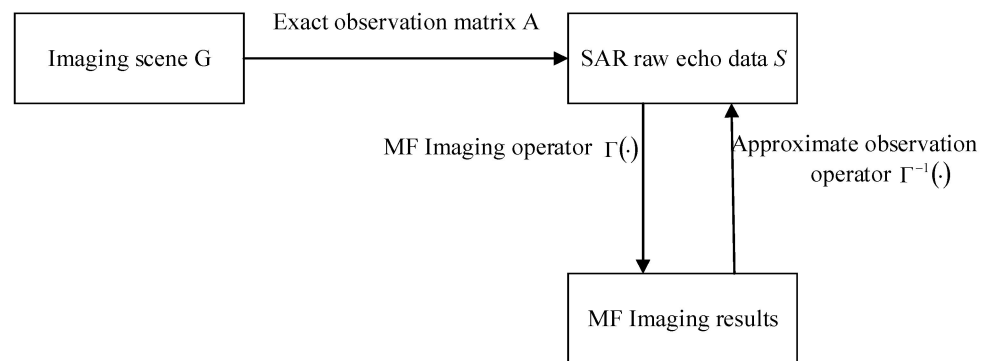


Figure 2. Schematic diagram of an approximate observation operator.

MF represents the matched filter imaging operator, and $\Gamma(\cdot)$ represents the conventional matched filtering algorithm. $\Gamma(\cdot)$ only contains the dot multiplication and FFT operation of the matrix, and its size is consistent with the size of the echo matrix, which has a high computational efficiency. Figure 2 shows that the $\Gamma(\cdot)$ inversion $\Gamma^{-1}(\cdot)$ can also be used to obtain the original SAR echo data, so $\Gamma^{-1}(\cdot)$ can be used instead of the accurate observation matrix A .

The CS-SAR reconstruction scene using the approximate observation operator is a problem of solving underdetermined equations. The scattering coefficient g of the scene can be obtained by solving the L1 norm regularization problem of Equation (9).

$$G = \underset{g}{\operatorname{argmin}} \left\{ \frac{1}{2} \|S - L \cdot \Gamma(G)\|_2^2 + \zeta \|G\|_1 \right\} \tag{9}$$

ζ represents the regularization coefficient, which is determined by the sparsity of the scene. L represents a sparse sampling matrix.

The essence of Equation (9) is an L1 norm regularization problem. Much practice has proved that the FIST method has a faster convergence rate than the IST method. Combined with the SFCWSAR model based on the approximate observation operator proposed in this paper, the FIST [25] method is selected to reconstruct scene G in this paper.

Let the maximum number of iterations be I_{\max} . G represents the scene to be reconstructed. The pseudo-code of the algorithm is shown in Algorithm 1.

Algorithm 1: SFCWSAR sparse imaging algorithm based on approximate observation

Initialization: $i = 0, V_0 = 0, t_0 = 1$,
 Reconstruction of scene scattering coefficient based on FIST
 $G_{i+1} = \underset{g}{\operatorname{argmin}} \left\{ \frac{1}{2} \|S - L \cdot \Gamma(G)\|_2^2 + \zeta \|G\|_1 \right\}$
 1: $V_{i+1} = \Psi_{\lambda, \delta}(V_i - \delta \Gamma(L \otimes (\Gamma^{-1}(G_i) - E)))$
 2: $t_{i+1} = \frac{1 + \sqrt{1 + 4t_i^2}}{2}$
 3: $G_{i+1} = V_{i+1} + \frac{t_i - 1}{t_{i+1}}(V_{i+1} - V_i)$
 4: $i = i + 1$,
 5: **if** $i = I_{\max}$, the solution is completed,
 6: **else** returns 1.

$\Psi_{\zeta \delta}(\cdot)$ represents the soft threshold operator, and δ is the search step size. $\delta = 1$ is taken in this model to ensure the convergence of the algorithm. The value of the parameter ζ is related to the sparsity K_0 of the imaging scene. The setting of $|V_i|^{(K_0)}$ in this model is the $\zeta = |V_i|^{(K_0)}$ K_0 th order of the magnitude of all elements of the matrix V_i in descending order of amplitude.

3.2. Range Migration Compensation in the Pulse Group

Selecting the approximate observation operator to replace the precise observation matrix used in the traditional CSSAR sparse reconstruction can reduce the amount of computer memory occupied by the algorithm and greatly improve the efficiency of the algorithm. Furthermore, for the special signal form of SFCWSAR, different pulses in the same pulse group appear to be discontinuous in the phase due to the relative motion between the radar and the target. The error mentioned above cannot be compensated using the exact observation operator, while the approximate observation operator is derived from the imaging algorithm. Therefore, the error mentioned above can be compensated using the approximate observation operator.

Firstly, the intra-group pulse range migration compensation algorithm of SFCWSAR proposed in document [26] is used to realize the intra-group sub-pulse motion compensation of the SFCWSAR raw echo data. The operation of the algorithm is defined as function C . Then, the above operation can be expressed as:

$$B = C(S) \tag{10}$$

where B represents the echo data after the range migration compensation in the pulse group. Then, the problem of solving the underdetermined system of equations in Equation (9) becomes:

$$G = \operatorname{argmin}_g \left\{ \frac{1}{2} \|B - L \cdot \Gamma(G)\|_2^2 + \zeta \|G\|_1 \right\} \quad (11)$$

3.3. SFCWSAR Sparse Imaging Model with an Approximate Observation Operator

Section 3.2 makes use of the characteristics of the approximate observation operator so that the SFCWSAR echo data after range migration compensation within the pulse group can be used for sparse reconstruction of the scene, but the sub-band signal needs to be windowed in the SFCWSAR imaging process. However, the inverse process of the imaging algorithm needs to be obtained when the approximate observation operator is established, and the inverse process of the windowing process is not easy to obtain, which affects the application of the approximate observation operator in SFCWSAR.

Based on this, an approximate observation model suitable for SFCWSAR is proposed in this paper. The model uses the synthetic bandwidth data as the echo data for imaging in the approximate observation model, thus cleverly skipping the establishment of the approximate observation operator. The specific idea is shown in Figure 3.

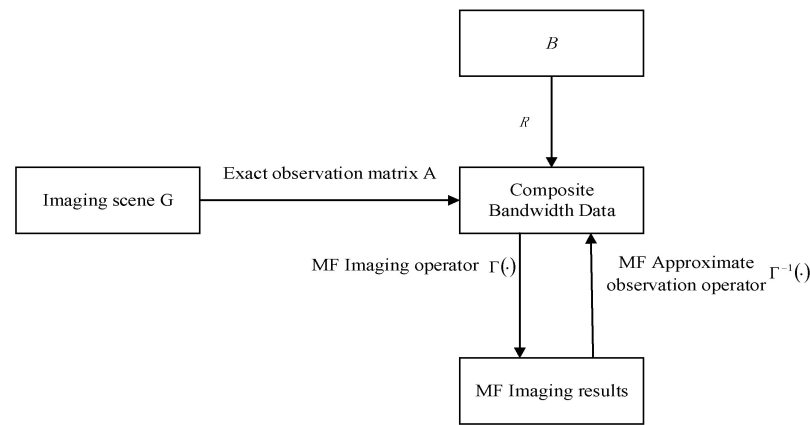


Figure 3. Approximate observation model of SFCWSAR.

The above operations in this paper are defined as function R . Combined with the SFCWSAR imaging process, the SFCWSAR bandwidth synthesis method proposed in this paper is expressed as a matrix:

$$E = R(B) \quad (12)$$

The matrix representation of the SFCWSAR imaging process based on the synthetic bandwidth data in this paper is:

$$G = \Gamma(E) = F_a(F_r^H(E \cdot H_c) \cdot H_a) \quad (13)$$

Then, the approximate observation operator of this model can be expressed as

$$E = \Gamma^{-1}(\cdot) = F_r(F_a^H(G) \cdot H_a^*) \cdot H_c^* \quad (14)$$

F_r represents the matrix form of FFT in the range direction. F_r^H represents the matrix form of IFFT in the range direction. F_a represents the matrix form of FFT in the azimuth direction. F_a^H represents the matrix form of IFFT in the azimuth direction. H_a represents the matrix form of the azimuth pulse compression. H_c represents the matrix form of the range migration correction factor. H_a^* represents the inverse operation of the azimuth pulse compression. H_c^* represents the inverse operation of the range migration correction.

The specific forms of H_a and H_c are:

$$H_a = \exp\left(2\pi f_d t + 1j\pi t^2 \cdot \frac{2v^2}{\lambda R}\right) \quad (15)$$

$$H_c = \exp(2\pi f_d t + 1j\pi t^2 \frac{2v^2 f_r}{\lambda R f_c}) \quad (16)$$

where f_d indicates the Doppler center frequency, f_r indicates the range frequency, and v indicates the carrier speed.

4. Analysis of the Memory Consumption and Computational Complexity of the Algorithm

4.1. Analysis of Algorithm Memory Consumption

Suppose that the observation scene is divided into the $P \times Q$ scattering unit in the range and azimuth directions. In the SFCWSAR echo data, there are N_r sampling points in the range direction and N_a sampling points in the azimuth direction. In the case of the same resolution and CS-SAR imaging based on accurate observation, the size of the observation matrix is $P \times Q \times N_r \times N_a$ complex numbers. The size of the observation matrix of CS-SFCWSAR based on the approximate observation operator is $N_r \times N_a$ complex numbers. Therefore, compared with the traditional CS-SAR imaging method, the method proposed in this paper significantly reduces the computer memory consumption and the demand for computer hardware.

4.2. Calculation Complexity Analysis of the Algorithm

Suppose the number of iterations required to complete the sparse reconstruction of the scene is M . A single iteration includes the following processes: the imaging process, approximate observation process, and fast soft threshold process. The computational complexity of the imaging process and approximate observation process is $O[N_r N_a \log_2(N_r N_a)]$, and the computational complexity of the fast soft threshold is $O(N_r N_a)$, so the computational complexity of CS-SFCWSAR is $O[MN_r N_a \log_2(N_r N_a)]$.

5. Doppler Center Frequency and Approximate Observation Operator

Section 3 discusses the sparse reconstruction algorithm of SFCWSAR based on approximate observation operator. The Doppler center frequency f_d is an important parameter for establishing the approximate observation operator.

5.1. Doppler Center Frequency

The synthetic aperture radar uses the principle of synthetic aperture to improve the azimuth resolution of the radar. Pulse compression techniques are used to improve the range resolution. During azimuth compression, the Doppler center frequency of the target echo must be accurately known to achieve matched filtering. The error of the Doppler center frequency will reduce the signal-to-noise ratio of the image, increase the azimuth ambiguity, and make the target position on the image shift, which will seriously reduce the imaging quality. For the SFCW sparse reconstruction model with an approximate observation operator, the Doppler center frequency, as an important parameter, deeply affects the accuracy of the approximate observation operator construction. The misalignment of the Doppler center frequency will lead to the mismatch between the theoretical model and the mathematical model, which will seriously affect the effect of sparse reconstruction.

However, the existing approximate observation sparse reconstruction models do not consider the difference between the Doppler center frequency value and the theoretical value caused by the non-ideal motion of the carrier aircraft. Furthermore, the phase error introduced by the non-ideal motion of the SAR carrier platform will lead to an estimation error. The Doppler center frequency can be calculated by measuring the relative position and velocity matrix centered between the target and the antenna, or it can be directly extracted from the SAR raw data. The SAR carrier is generally equipped with a navigation and measurement system to detect the fast and slow variation of the antenna phase center and the in-plane and non-planar components of the disturbance and to compensate accordingly. However, high-precision inertial navigation equipment will increase the hardware cost of the system, and some micro SAR systems cannot carry

inertial navigation equipment with a large volume and weight. The data-driven autofocus algorithm estimates the phase error from the echo data. Although it increases the complexity of the algorithm, it can meet the requirements of high-resolution imaging without increasing the cost of system hardware [27].

Based on the above problems, this paper proposes an SFCWSAR sparse reconstruction method using sub-band data to estimate Doppler parameters and modify the approximate observation operator. First, the method sets the sampling matrix so that the sub-band echo data under the full sampling condition can be obtained simultaneously when the undersampled SFCWSAR echo data are obtained. Then, the Doppler parameters caused by the carrier’s non-ideal motion are corrected by using the sub-band echo data under the full sampling condition. The approximate observation operator is constructed by using the modified Doppler center frequency. Finally, SFCWSAR sparse reconstruction is realized by using the modified approximate observation operator.

5.2. Setting of the Algorithm Sampling Matrix

In order to obtain the complete sub-pulse data while obtaining the sparse sampling data, the sparse sampling matrix in this paper is set to three types: A, B, and C. The three are satisfied, where B is the sampling matrix for obtaining the complete sub-pulse echo data and C is the matrix for the sparse sampling of the data from the whole echo, except for the complete sub-pulse echo. A can be obtained by computing C and B. The schematic diagrams of the three matrices, A, B, and C, are shown in Figure 4.

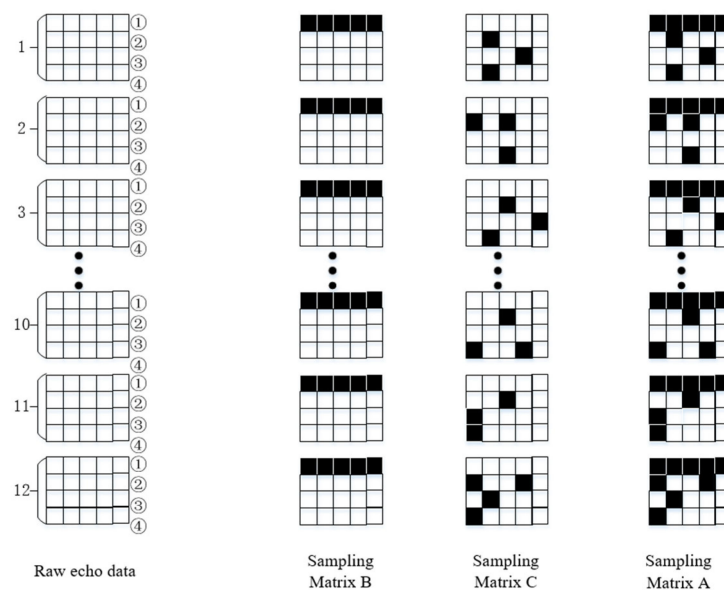


Figure 4. Schematic diagram of the three sampling matrices of the SFCWSAR approximate observation operator.

Using the sampling matrix shown in Figure 4, to facilitate the description of SFCWSAR data, the number of azimuth pulse groups is set to 12, the number of subpulses per pulse is set to 4, and the number of range sampling points is set to 5.

We can obtain the sub-band echo data under full sampling conditions while obtaining the sparse sampling matrix. Therefore, the narrowband echo data under full sampling can be used to estimate the Doppler center frequency.

5.3. Doppler Center Frequency Estimation

Because it is often difficult for the speed and detection accuracy of the equipment to meet the requirements of high-resolution imaging, in order to obtain an accurate Doppler center frequency, this algorithm chooses to use sub-band echo data to estimate the Doppler center.

Doppler center frequency estimation methods mainly include the frequency domain estimation method and time domain estimation method.

Due to the small size of the UAV platform, it is easily affected by airflow disturbance and its mechanical vibration. Therefore, there are approximately periodic changes in the Doppler center of the azimuth signal, so the phase-based time domain correlation method cannot accurately estimate the Doppler center frequency. In addition, the influence of the beam-pointing jitter on the amplitude of the azimuth signal is much smaller than the influence on the signal phase. Therefore, the amplitude-based clutter locking method is applied to estimate the Doppler center in this paper [27].

The specific method is: first, obtain the azimuth Doppler spectrum of the echo of the sub-band signal under the full sampling condition, and the center frequency of the azimuth signal is approximately equal to its spectrum center of gravity [28]. Therefore, the center frequency can be estimated by taking the azimuth signal of a range gate to calculate its spectrum center of gravity. However, in fact, the front end and back end of the acquired azimuth signal inevitably contain some incomplete Doppler histories. These incomplete Doppler histories constitute an important source of estimation bias. In order to improve the estimation accuracy, the average power spectrum of all or part of the azimuth signals of the range gate can be used. Finally, the energy center of the above power spectrum can be found. By retrieving the points with equal spectral energy integrals on both sides, the frequency corresponding to this center is the Doppler center frequency estimated by the clutter locking method.

Using the above method, the Doppler center frequency is estimated as f_{dc} using the narrow band sub-pulse, and f_{dc} is substituted into the approximate observation operator. The modified approximate observation operator is recorded as Γ_c . Γ_c will be used for the sparse reconstruction of the scene.

5.4. Algorithm Pseudocode and Flow Chart

Section 5.4 further explains the algorithm in this paper by using the algorithm pseudo code and flow chart.

The pseudo code of the algorithm 2 proposed in this paper is shown in the following Algorithm 2:

Algorithm 2 Sparse reconstruction algorithm based on range migration compensation and Doppler center frequency correction in the pulse group

Step 1:

1: For SFCWSAR echo data, use sampling matrix A to conduct sparse sampling for the echo. The narrowband echo data EB and the undersampled SFCWSAR echo data EA are obtained under the condition of full sampling.

2: The EB is used to estimate the Doppler center frequency f_d , and the estimated f_{dc} is used to modify the approximate observation operator to obtain the modified approximate observation operator Γ_c .

3: The echo data E is obtained by range migration compensation and bandwidth synthesis within the pulse group for EA .

Step 2: Initialization: $i = 0, V_0 = 0, t_0 = 1,$

Reconstruction of scene scattering coefficient based on FIST

$$G_{i+1} = \underset{g}{\operatorname{argmin}} \left\{ \frac{1}{2} \|E - L \cdot \Gamma_c(G)\|_2^2 + \zeta \|G\|_1 \right\}$$

$$4: V_{i+1} = \Psi_{\lambda, \delta}(V_i - \delta \Gamma(L \otimes (\Gamma_c^{-1}(G_i) - E)))$$

$$5: t_{i+1} = \frac{1 + \sqrt{1 + 4t_i^2}}{2}$$

$$6: G_{i+1} = V_{i+1} + \frac{t_i - 1}{t_{i+1}}(V_{i+1} - V_i)$$

$$7: i = i + 1,$$

8: **if** $i = I_{\max}$, the solution is completed,

9: **else** returns 4.

The algorithm flow chart is shown in Figure 5.

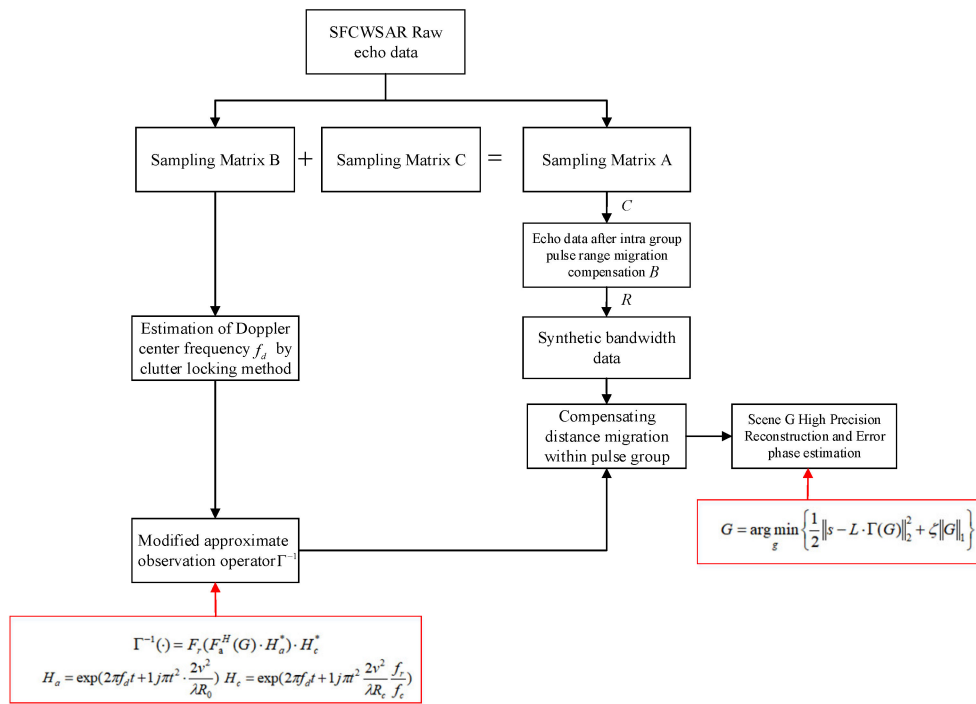


Figure 5. Flow chart of the sparse reconstruction algorithm based on the approximate observation operator SFCWSAR to compensate for the range migration within the pulse group and correct the Doppler Center Frequency.

6. Measured Data Verification

In this section, the simulation and measured data are used to verify the effectiveness of the proposed algorithm. Section 6.1 presents the simulation data verification. The approximate observation operator is used instead of the exact operator to realize the correction of the range migration within the SFCWSAR pulse group and to realize the sparse reconstruction of the scene under the condition of an undersampling rate. Section 6.2 shows the verification of the measured data, and the measured data of the side-view airborne SFCWSAR is selected to verify the proposed algorithm. Using the sub-band echo data under the full sampling condition mainly realizes the correction of the Doppler center and improves the sparse reconstruction effect. Furthermore, the flight speed of the carrier aircraft in the measured data is low, and the range migration within the pulse group can be ignored by calculation, which will not affect the imaging results. Therefore, only the Doppler operator correction approximate observation operator part of the proposed algorithm is verified in Section 6.2.

6.1. Simulation Data Verification

The parameters of the simulation experiment system are shown in Table 1.

Table 1. Simulation Experiment SFCWSAR system parameters.

Carrier Frequency/GHz	Each Sub-Bandwidth/MHz	Pulse Width/ μ s	The Flight Speed of the Carrier Aircraft/m/s	The Number of Pulses per Group	Range Sampling Rate/MHz	Frequency Hopping Spacing/MHz
5	200	1.5	200	2	420	200

A total of 30 point targets are designed in the experimental scene, and their geometric distribution is shown in Figure 6.

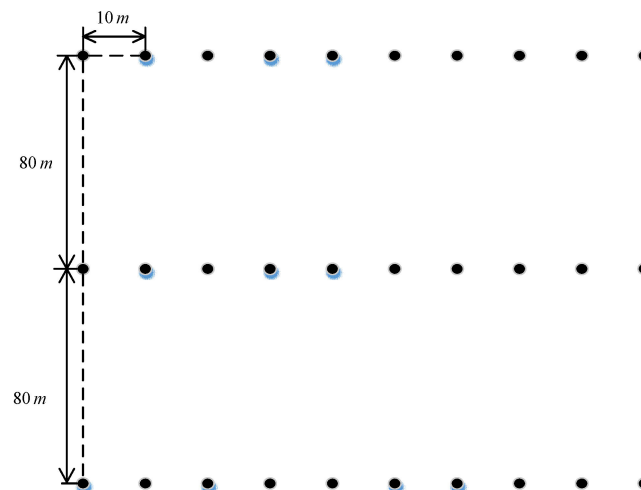


Figure 6. Geometric distribution of point targets.

During the experiment, the measured data are extracted in the azimuth direction, and the echo data extraction rate is ζ . $\zeta = 1$ represents the fully sampled echo data. The decimation rate is chosen to be 0.5. When the echo decimation rate is equal to 0.5, the result of the imaging processing directly on the echo data under the undersampling condition is shown in Figure 7.

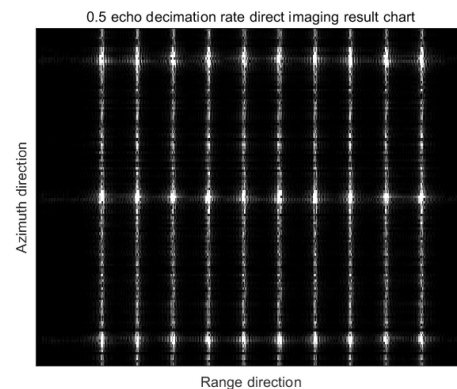


Figure 7. Direct imaging result of the 0.5 echo extraction rate.

Figure 7 shows that when the echo decimation rate is 0.5, the echo data under the undersampling condition is directly imaged, and the image quality is degraded due to the noise caused by the undersampling. Furthermore, the phase discontinuity caused by the relative motion of the radar and the target within the pulse group broadens the main lobe and even causes the divergence distortion of the waveform, which further reduces the image quality.

The algorithm proposed in this paper uses the approximate observation operator to replace the precise observation operator in the traditional CSSAR to sparsely reconstruct the scene from the data under the above-mentioned undersampling condition. The algorithm that directly uses the approximate observation operator to realize the sparse reconstruction of the scene is called Algorithm 1. The algorithm proposed in this paper that first corrects the range migration within the SFCWSAR pulse group and then uses the approximate observation operator to perform sparse imaging processing is called Algorithm 2. The sparse reconstruction results of each algorithm and the enlarged area in the red box in the results are shown in Figure 8.

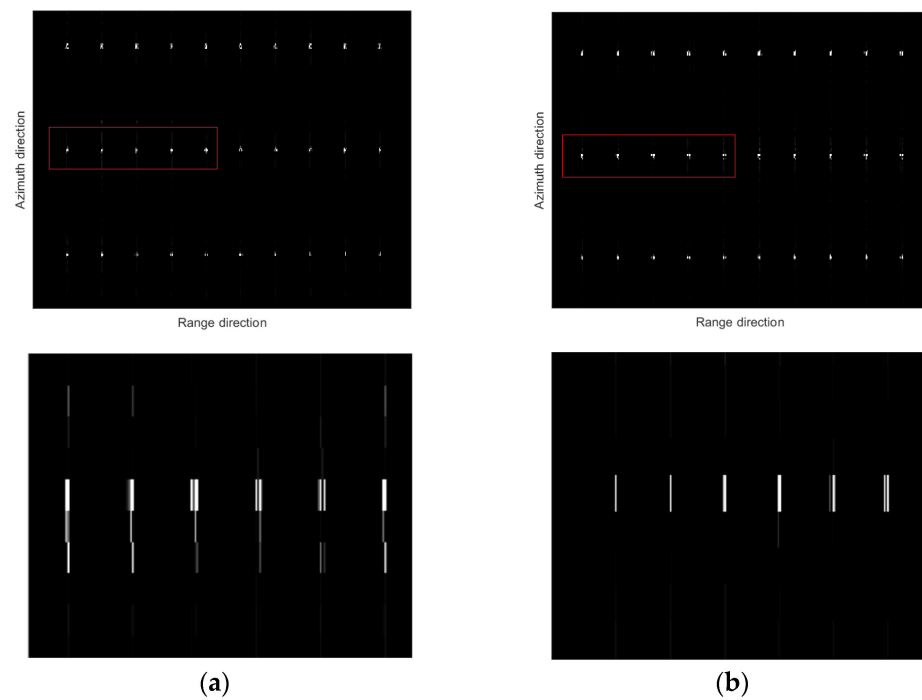


Figure 8. The sparse reconstruction diagram of each algorithm with a 0.5 echo extraction rate: (a) Algorithm 1, (b) Algorithm 2.

As shown in Figure 8, the approximate observation operator is selected for CSSAR sparse reconstruction, which can realize scene reconstruction with a low data volume. For CSSFCWSAR, using the approximate observation operator can greatly reduce the memory usage of the computer when the algorithm is running and greatly improve the running efficiency of the algorithm. In addition, for the special signal form of SFCWSAR, different pulses in the same pulse group appear discontinuous in the phase due to the relative motion between the radar and the target. The phase error can be compensated by adopting the approximate observation operator. Figure 8 shows the sparse reconstruction map of the scene and an enlarged view of the red boxed area in the target scene, and Algorithm 2 shows a better sparse reconstruction effect. Since Algorithm 1 does not compensate for the phase error between different pulses in the same pulse group, the target range decreases in amplitude, the main lobe broadens, and the waveform diverges and distorts, resulting in a corresponding decrease in the reconstruction effect of the point target. Algorithm 2 uses the approximate observation operator to compensate for the phase errors of different pulses in the same pulse group and then further realizes the sparse reconstruction of the target. Since the error phase is compensated, the sparse reconstruction result of Algorithm 2 is significantly improved compared with Algorithm 1. The algorithm in this paper achieves high-precision sparse reconstruction of the target scene, reduces the computer memory footprint, and improves the efficiency of the algorithm simultaneously.

6.2. Measured Data Verification

In this section, the effectiveness of the proposed algorithm is verified by the airborne SFCWSAR measured data. The system parameters are shown in Table 2.

Table 2. SFCWSAR system parameters.

Carrier Frequency/GHz	Each Sub-Bandwidth/MHz	Pulse Width/ μ s	The Flight Speed of the Carrier Aircraft/m/s	The Number of Pulses per Group	Range Sampling Rate/MHz	Frequency Hopping Spacing/MHz
15.72	50	3	17.6	24	160	40

The exact observation operator in the traditional sparse compressed sensing model is replaced by the exact observation operator. The extraction rates are selected as 0.3, 0.5, and 0.7, respectively. In order to compare the convergence speed and accuracy of each algorithm, the number of iterations is unified to 10 times. The sparsity is set to 1572 (this parameter determines the FIST threshold). The algorithm that does not correct the Doppler center frequency in the SFCWSAR approximate observation operator is called Algorithm 1, and the algorithm in this paper is called Algorithm 2. Algorithm 1 and Algorithm 2 are used to image the SFCWSAR data, respectively. Due to the influence of the motion error, the image is defocused. In order to compare the sparse reconstruction performance of each algorithm, the sparsely sampled SFCWSAR data, after sparse reconstruction, adopted the sparse autofocus algorithm [16] to perform motion compensation on the SAR data. Algorithm 2 selects the twelfth sub-pulse in each pulse group as the fully sampled narrow band pulse signal, and the sub-pulse signal accounts for 4.1% of the original echo data. It should be noted that although the algorithm obtains the narrow band pulse signal under the full sampling condition, the undersampling rate of the overall signal is consistent with the comparison algorithm.

The sparse reconstruction maps of each algorithm are shown in Figures 9–11. The imaging scene is a field in China. Figure 11 shows the sparse reconstruction map and the enlarged area map in the red box.

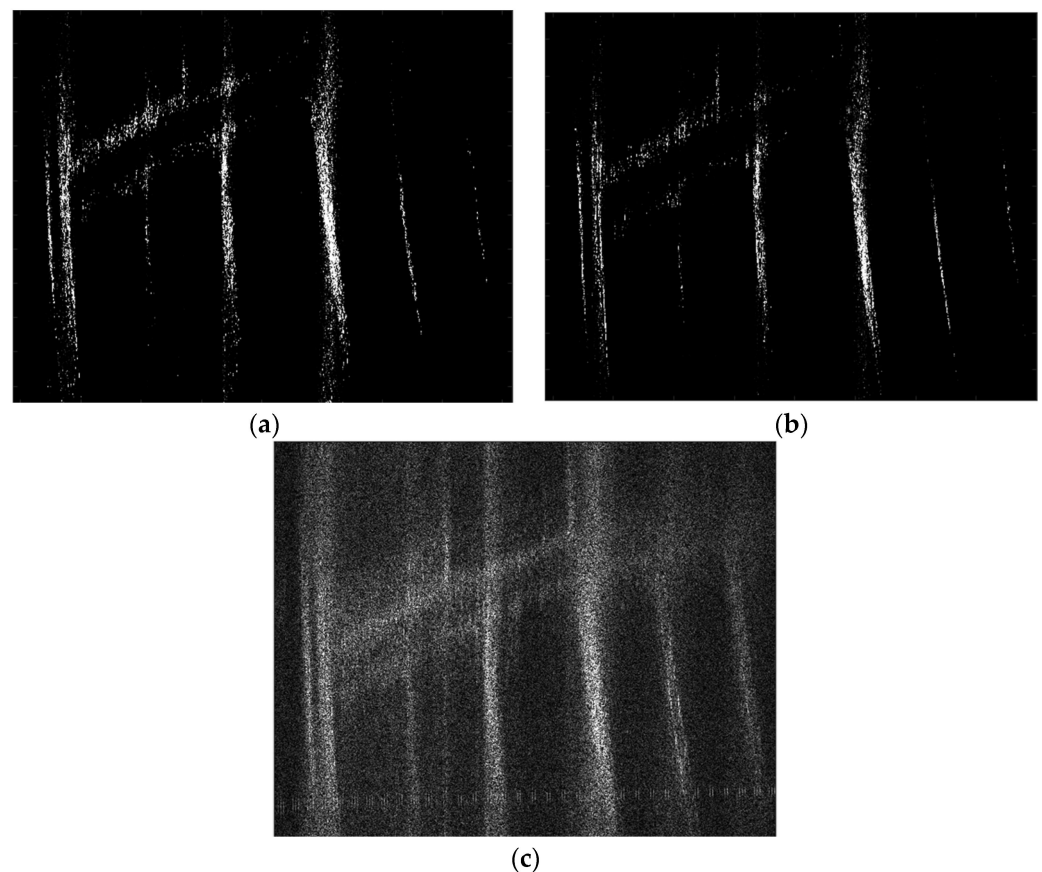


Figure 9. The imaging results of each algorithm with an undersampling rate of 0.3: (a) Algorithm 1, (b) Algorithm 2, (c) Direct imaging.

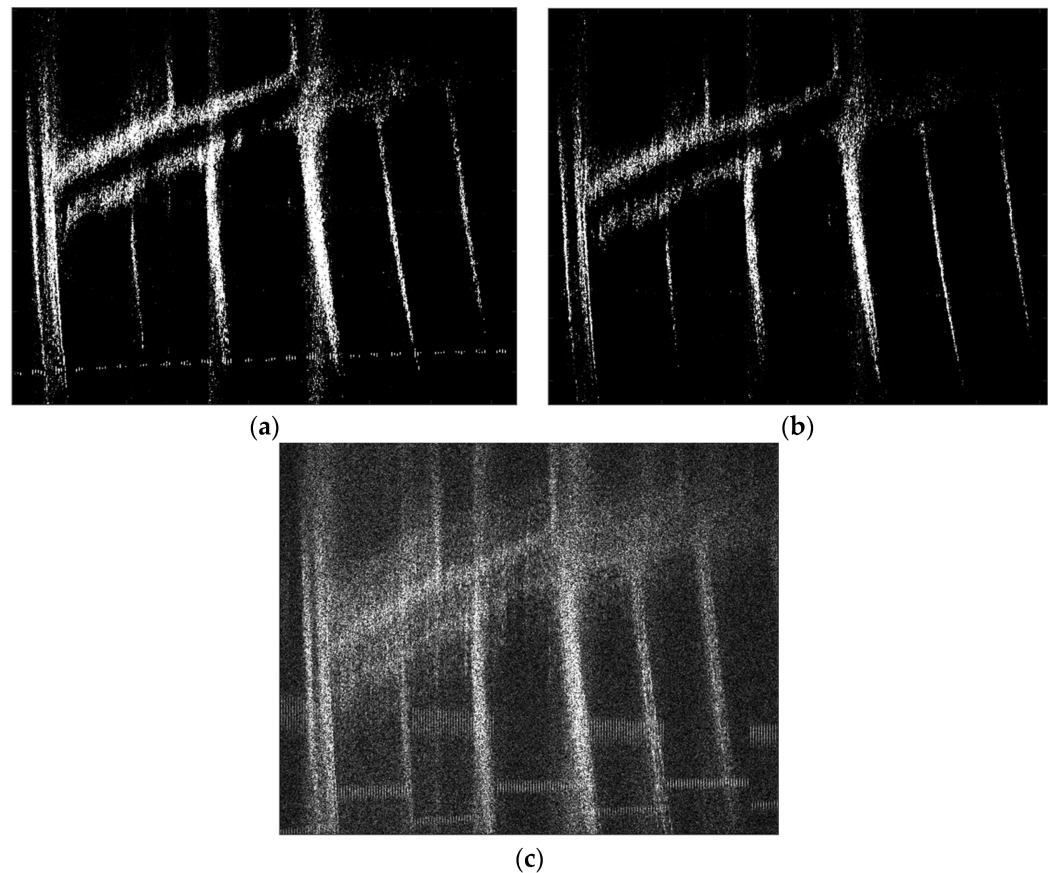


Figure 10. Imaging results of each algorithm with an undersampling rate of 0.5: (a) Algorithm 1, (b) Algorithm 2, (c) Direct imaging.

Figures 9c, 10c and 11c show that the data under the undersampling condition are directly imaged, and the noise caused by the undersampling leads to a significant decrease in the quality of the imaging results. By observing (a) and (b) of Figures 9–11, it can be seen that using the approximate observation operator instead of the precise observation operator can use the data under the undersampling condition to reconstruct the scene with high precision. Using approximate observation operators can greatly reduce the amount of computer memory occupied by the algorithm when it is running and improve the running efficiency of the algorithm.

By comparing and observing (a) and (b) in Figures 9–11, Algorithm 2 has a better sparse reconstruction effect than Algorithm 1. The reason for the result is that the approximate observation operator is derived from the imaging algorithm, and the Doppler center, as the core parameter of the imaging algorithm, is naturally an important parameter for the establishment of the approximate observation operator. However, the non-ideal movement of the carrier aircraft in the air, including the position deviation of the carrier aircraft from the ideal track, the change in the center of the radar beam, or the errors caused by the mechanical vibration of the carrier aircraft itself, can cause the Doppler center frequency to shift. Algorithm 1 selects the Doppler center frequency obtained by the theoretical calculation to construct the approximate observation operator. The mismatch of the Doppler center frequency will reduce the signal-to-noise ratio of the image, increase the azimuth ambiguity, and make the target on the image. The position is offset. The above reasons cause the error between the approximate observation operator and the theoretical imaging model. Therefore, the sparse reconstruction quality of Algorithm 1 needs to be improved. Algorithm 2 uses the sub-band data under full sampling conditions to estimate the Doppler center frequency using the clutter locking method. Furthermore, the estimated Doppler center frequency is used to approximate the construction of the

observation operator, which improves the reconstruction algorithm and the mathematical model. Therefore, it has a better sparse reconstruction effect.

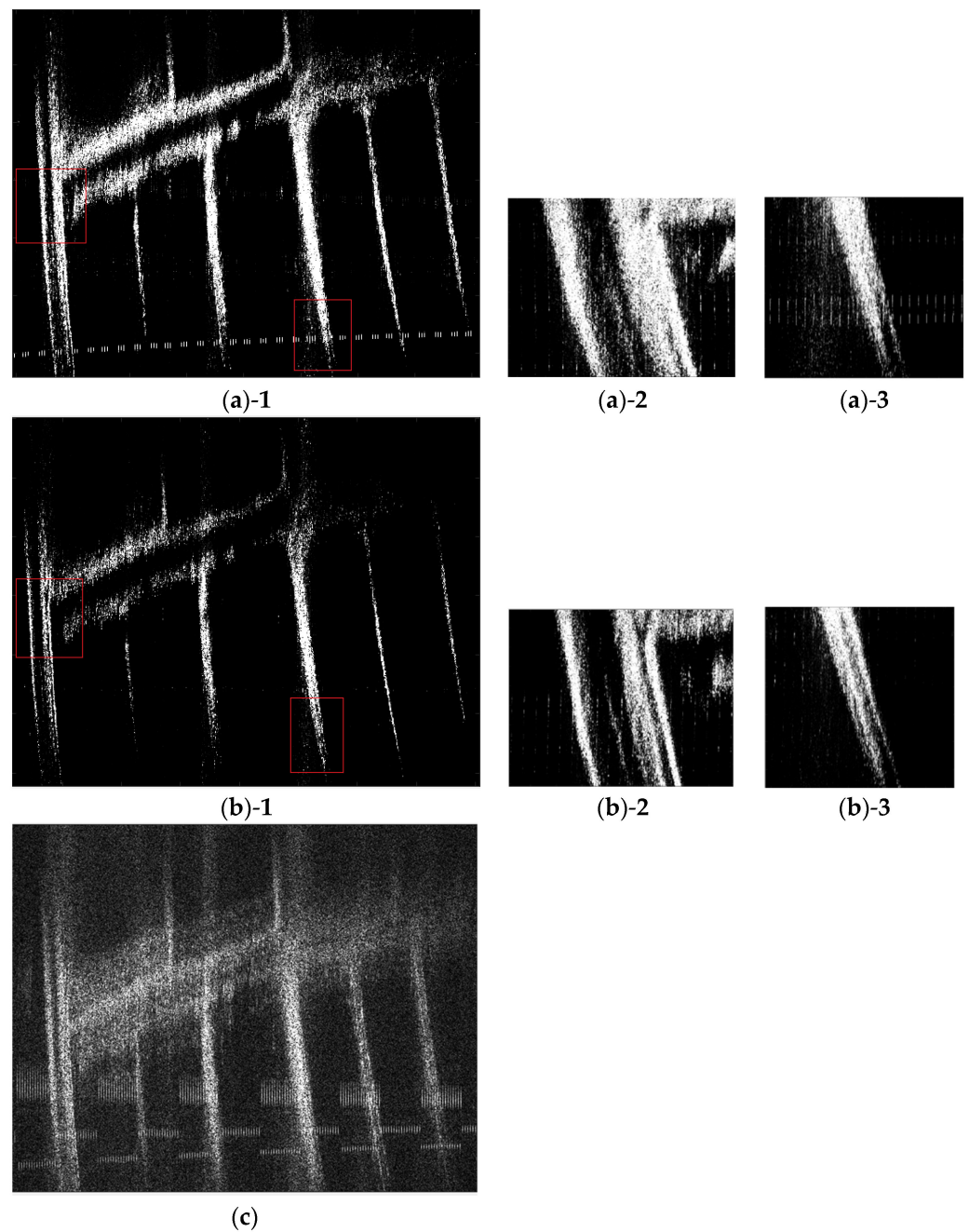


Figure 11. Imaging results of each algorithm with an undersampling rate of 0.7: (a) Algorithm 1, (b) Algorithm 2, (c) Direct imaging.

After obtaining the Doppler spectrum of the echo, the average power spectrum of all range units in the scene is calculated. The results are shown in Figure 12. The estimated value of the Doppler center frequency can be calculated to be 81.90hz. The theoretical value of the SAR Doppler center frequency in the case of the frontal view is 0. If the Doppler center frequency is not estimated directly, the Doppler center is 0 for the construction of the approximate observation operator. The above error will cause the quality of the sparse reconstruction results to decrease.

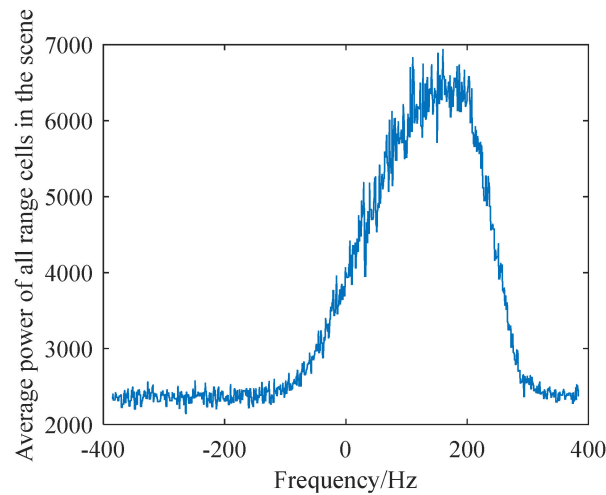


Figure 12. Average power spectrum of all range cells in the scene.

The above images are judged by the entropy of the image. The entropy of the image is expressed as the average number of bits of the gray level set of the image, which describes the average information amount of the image source. It is generally believed that a smaller entropy value of the image indicates a better focusing quality of the SAR image.

The change in the entropy value of each method in 10 iterations is shown in Figure 13. The final entropy value of the image convergence of each algorithm under each sampling rate after 10 iterations is shown in Table 3.

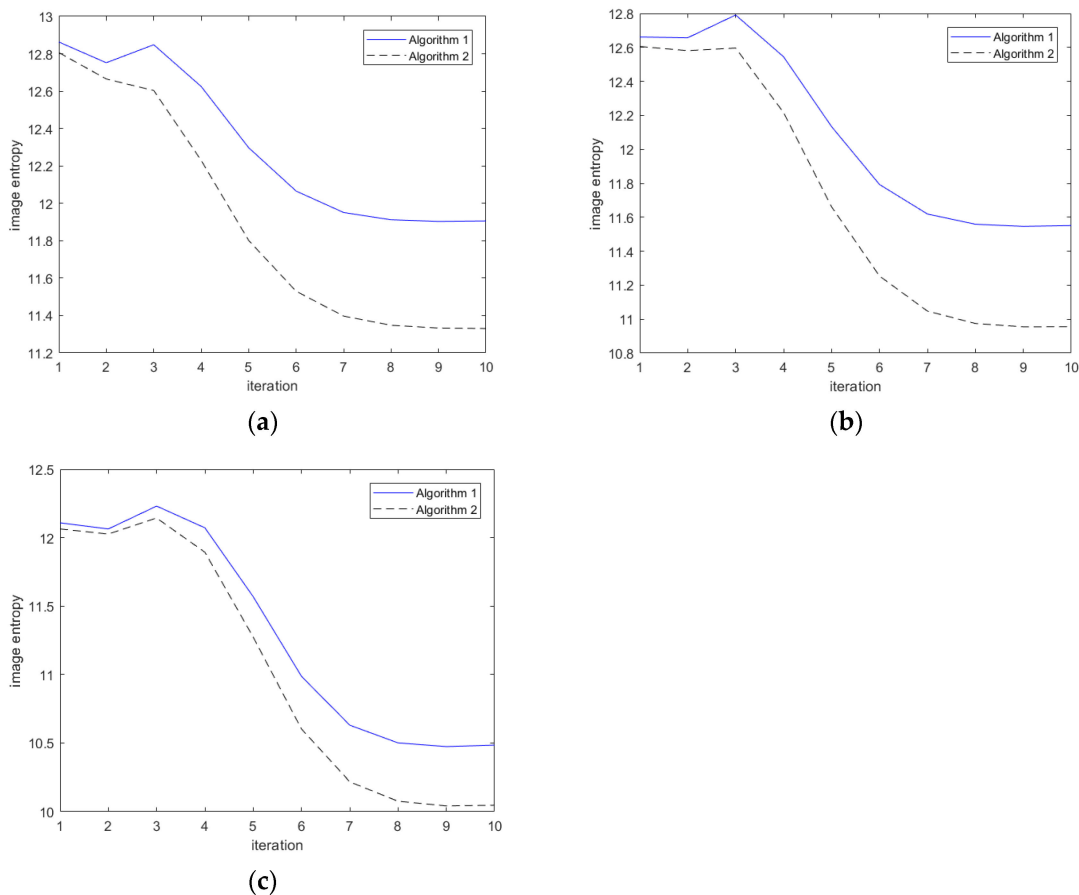


Figure 13. Entropy value change curve of each method in 10 iterations: (a) 0.7 echo extraction rate, (b) 0.5 echo extraction rate, (c) 0.3 echo extraction rate.

Table 3. The final entropy value of the image convergence after 10 iterations of each algorithm under each sampling rate.

	0.3	0.5	0.7
Algorithm 1	10.48	11.55	11.90
Algorithm 2	10.05	10.95	11.35

Figure 13 and Table 3 show that, under the same undersampling rate, the initial entropy value of the image of Algorithm 2 and the final entropy value of image convergence are lower than those of Algorithm 1. The results show that Algorithm 2 has a better sparse reconstruction effect than Algorithm 1. Although Algorithm 1 can reconstruct the scene, it does not consider the impact of the non-ideal motion of the carrier on the Doppler center. Therefore, the sparse reconstruction effect is affected, and the target position in the scene is offset. This paper selects the sparse autofocus algorithm proposed in a previous study [16] to compensate for the phase error in SAR data during the experiment. However, the sparse reconstruction effect cannot be further improved due to the errors in the parameters of the approximate observation operator itself, and the inherent errors of the algorithm model cannot be compensated. For Algorithm 2 proposed in this paper, the approximate observation operator matches the mathematical model of the actual imaging algorithm better due to the correction of the deviation of the Doppler parameter. The accurate Doppler center frequency improves the signal-to-noise ratio and image resolution, and the corresponding Algorithm 2 has a better sparse reconstruction effect. The iterative entropy from the image and the converged final entropy of Algorithm 2 are significantly better than those of Algorithm 1.

7. Concluding Remarks

The approximate observation operator is derived from the inverse operation of the imaging algorithm. In this paper, a sparse reconstruction algorithm of SFCWSAR based on the approximate observation operator is proposed, which greatly reduces the occupation of computer memory when the algorithm runs and realizes the range migration compensation within the SFCWSAR pulse group. On the other hand, the algorithm modifies the Doppler center frequency, an important parameter of the approximate observation operator, and increases the matching degree between the approximate observation operator and the actual imaging process, further improving the scene reconstruction effect. The measured data show that the algorithm proposed in this paper can effectively reconstruct the scene with high precision, and the computational efficiency is greatly improved. The phase error caused by the non-ideal motion of the carrier will cause serious defocus in the reconstructed scene. The next step will be to study the problem of CSSAR motion compensation.

Author Contributions: Writing—original draft preparation, X.H.; writing—review and editing, Y.M. All authors have read and agreed to the published version of the manuscript.

Funding: This research received no external funding.

Conflicts of Interest: The authors declare no conflict of interest.

References

1. Tang, S.; Zhang, L.; Guo, P.; Liu, G.; Zhang, Y.; Li, Q.; Gu, Y.; Lin, C. Processing of monostatic SAR data with general configurations. *IEEE Trans. Geosci. Remote Sens.* **2015**, *53*, 6529–6546. [[CrossRef](#)]
2. Prats-Iraola, P.; Scheiber, R.; Rodriguez-Cassola, M.; Mittermayer, J.; Wollstadt, S.; De Zan, F.; Brautigam, B.; Schwerdt, M.; Reigber, A.; Moreira, A. On the processing of very high resolution spaceborne SAR data. *IEEE Trans. Geosci. Remote Sens.* **2014**, *52*, 6003–6016. [[CrossRef](#)]
3. Dekker, P.L.; Rodriguez-Cassola, M.; De Zan, F.; Krieger, G.; Moreira, A. Correlating synthetic aperture radar (CoSAR). *IEEE Trans. Geosci. Remote Sens.* **2015**, *54*, 2268–2284. [[CrossRef](#)]
4. Moreira, A.; Prats-Iraola, P.; Younis, M.; Krieger, G.; Hajnsek, I.; Papathanassiou, K.P. A tutorial on synthetic aperture radar. *IEEE Geosci. Remote Sens. Mag.* **2013**, *1*, 6–43. [[CrossRef](#)]

5. Chen, J.; Xing, M.; Sun, G.-C.; Li, Z. A 2-D space-variant motion estimation and compensation method for ultrahigh-resolution airborne stepped-frequency SAR with long integration time. *IEEE Trans. Geosci. Remote Sens.* **2017**, *55*, 6390–6401. [[CrossRef](#)]
6. Berens, P. SAR with ultra-high range resolution using synthetic bandwidth. *Proc. IEEE Int. Geosci. Remote Sens. Symp.* **2003**, *3*, 1752–1754.
7. Li, J.; Chen, J.; Liu, W.; Wang, P.; Li, C. A synthetic bandwidth method for high-resolution SAR based on PGA in the range dimension. *Sensors* **2015**, *15*, 15339–15362. [[CrossRef](#)]
8. Balon, S.; Moutahaan, K.; Heng, C.-H.; Chen, Z.N. A C-band FMCW SAR transmitter with 2-GHz bandwidth using injection-locking and synthetic bandwidth techniques. *IEEE Trans. Microw. Theory Tech.* **2018**, *66*, 5095–5105. [[CrossRef](#)]
9. Woodward, P.W. *Probability and Information Theory, with Application to Radar*; Pergamon: New York, NY, USA, 1953.
10. Bi, H.; Bi, G.; Zhang, B.; Hong, W.; Wu, Y. From theory to application: Real-time sparse SAR imaging. *IEEE Trans. Geosci. Remote Sens.* **2019**, *58*, 2928–2936. [[CrossRef](#)]
11. Zhang, B.; Hong, W.; Wu, Y. Sparse microwave imaging: Principles and applications. *Sci. China Inf. Sci.* **2012**, *55*, 1722–1754. [[CrossRef](#)]
12. Zhang, L.; Xing, M.; Qiu, C.-W.; Li, J.; Shen, J.; Bao, Z. Resolution enhancement for inversed synthetic aperture radar imaging under low SNR via improved compressive sensing. *IEEE Trans. Geosci. Remote Sens.* **2010**, *48*, 3824–3838. [[CrossRef](#)]
13. Çetin, M.; Stojanović, I.; Önhon, N.Ö.; Varshney, K.; Samadi, S.; Karl, W.C.; Willsky, A.S. Sparsity-driven synthetic aperture radar imaging: Reconstruction, autofocusing, moving targets, and compressed sensing. *IEEE Signal Process Mag.* **2014**, *31*, 27–40. [[CrossRef](#)]
14. Yang, L.; Li, P.; Li, H.; Fang, C. Robust and efficient general SAR image sparse feature enhancement algorithm. *Acta Electron. Sin.* **2019**, *41*, 2826–2835.
15. Ender, J. A brief review of compressive sensing applied to radar. In Proceedings of the 2013 14th International Radar Symposium (IRS), Dresden, Germany, 19–21 June 2013; pp. 3–16.
16. Li, B.; Liu, F.; Zhou, C.; Lv, Y.; Hu, J. Phase error correction for approximated observation-based compressed sensing radar imaging. *Sensors* **2017**, *17*, 613. [[CrossRef](#)] [[PubMed](#)]
17. Fang, J.; Xu, Z.; Zhang, B.; Hong, W.; Wu, Y. Fast compressed sensing SAR imaging based on approximated observation. *IEEE J. Sel. Top. Appl. Earth Obs. Remote Sens.* **2013**, *7*, 352–363. [[CrossRef](#)]
18. Dong, X.; Zhang, Y. A novel compressive sensing algorithm for SAR imaging. *IEEE J. Sel. Top. Appl. Earth Obs. Remote Sens.* **2013**, *7*, 708–720. [[CrossRef](#)]
19. Bi, H.; Zhang, B.; Zhu, X.X.; Hong, W. Azimuth-range decouple-based L1 regularization method for wide ScanSAR imaging via extended chirp scaling. *J. Appl. Remote Sens.* **2017**, *11*, 015007. [[CrossRef](#)]
20. Bi, H.; Zhang, B.; Zhu, X.X.; Jiang, C.; Hong, W. Extended chirp scaling-baseband azimuth scaling-based azimuth-range decouple L1 regularization for TOPS SAR imaging via CAMP. *IEEE Trans. Geosci. Remote Sens.* **2017**, *55*, 3748–3763. [[CrossRef](#)]
21. Xu, Z.; Wei, Z.; Wu, C.; Zhang, B. Multichannel sliding spotlight SAR imaging based on sparse signal processing. In Proceedings of the IGARSS 2018-2018 IEEE International Geoscience and Remote Sensing Symposium, Valencia, Spain, 22–27 July 2018; pp. 3703–3706.
22. Raney, R.K.; Vachon, P.W. A phase preserving SAR Processor. In Proceedings of the IGARSS'89 12th Canadian Symposium on Remote Sensing, Vancouver, BC, Canada, 10–14 July 1989; pp. 2588–2591.
23. Moreira, J.R. A new method of aircraft motion error extraction from radar raw data for real time motion compensation. *IEEE Trans. Geosci. Remote Sens.* **1990**, *28*, 620–626. [[CrossRef](#)]
24. Li, G.; Ma, Y.; Dong, J. Total variation regularization-based compressed sensing synthetic aperture radar imaging. *J. Appl. Remote Sens.* **2018**, *2*, 045017. [[CrossRef](#)]
25. Beck, A.; Teboulle, M. A fast iterative shrinkage-thresholding algorithm for linear inverse problems. *SIAM J. Imaging Sci.* **2009**, *2*, 183–202. [[CrossRef](#)]
26. Xu, Z. *Research on Key Technologies of Ultra High Resolution Airborne sar Imaging*; Ma topic; Nanjing University of Aeronautics and Astronautics: Nanjing, China, 2018.
27. Liu, Y. *Doppler Parameter Estimation and Imaging Algorithm Research of Airborne SAR Measured Data*; Ma topic; Harbin Institute of Technology: Harbin, China, 2006.
28. Wang, J.; Guo, Z. *Research on Digital Clutter Locking of Airborne SAR*; China Electronics Society: Hangzhou, China, 1998.

Disclaimer/Publisher's Note: The statements, opinions and data contained in all publications are solely those of the individual author(s) and contributor(s) and not of MDPI and/or the editor(s). MDPI and/or the editor(s) disclaim responsibility for any injury to people or property resulting from any ideas, methods, instructions or products referred to in the content.